



Virtual Porosimeter

Eduard Vergés¹, Dolors Ayala², Sergi Grau³ and Dani Tost⁴

¹CREB/IBEC Polytechnic University of Catalonia, everges@lsi.upc.edu

²CREB/IBEC Polytechnic University of Catalonia, dolorsa@lsi.upc.edu

³CREB/IBEC Polytechnic University of Catalonia, sgrau@lsi.upc.edu

⁴CREB/IBEC Polytechnic University of Catalonia, dani@lsi.upc.edu

ABSTRACT

Recently, the term Bio-CAD has appeared to refer to the modeling of biological processes. This work focuses on the analysis of structural properties such as porosity of bioimplants for bone reconstruction. Specifically, we present a method that, using 3D microCT images, simulates the behavior of a porosimeter, i.e. an instrument to measure the porous structure of samples. After segmentation, we apply a process, based on connected component labeling and skeleton computation, which produces a result comparable to the real porosimeter experiment.

Keywords: bio-CAD modeling, 3D digital topology, pore quantification.

DOI: 10.3722/cadaps.2008.557-564

1. INTRODUCTION

In recent years, the spectacular development of bioengineering has yield to the apparition of a new application field of Computer-Aided-Design, the Bio-CAD, aimed at the design of new models for biological structures and simulation methods for biological processes. One of the most active areas in bioengineering is the design of new bioactive materials for bone repair, such as hydroxylapatite that promotes osseointegration. They can be implanted into damaged bones, where they stimulate bone formation. The characterization of the bioimplants not only depends on the chemical composition of the bioimplant but also on its topological structure. Specifically, bone ingrowth occurs through the pores of the implants where blood can flow. Therefore, the analysis of the pores volume, their distribution and their interconnectivity is of paramount importance for the design of biomaterials. Another related and relevant application is the analysis of structural parameters as porosity and connectivity of trabecular bone samples, in order to predict bone fracture.

Currently, the physical device used to measure the porosity of the materials is the porosimeter. Porosimeters measure the intrusion volume of a fluid through a core sample of the material as a function of the pressure applied to the fluid. Pressure yields pore diameters. Usually the fluid used is mercury, but for hydrophobic samples, water-based porosimeters can be used. Porosimeters provide the volume of pores connected to the exterior (*Effective Porosity*) and the distribution of pores diameters. A drawback of real porosimetry is that the analyzed sample can become deformed at high pressures. Besides, porosimeters do not measure other relevant parameters related to porosity, such as the volume of pores not connected to the exterior (internal pores or cavities) and the interconnectivity between pores. For such measurements, BioCAD tools have been designed, based on the analysis of 3D images of a sample scanned with a medical imaging device, generally a microCT. Given a 3D voxel model of CT-scanned sample, it is possible to measure the *Total Porosity* of the material by counting the number of empty voxels. Then, the connected components of the pores space can be separated and a seed-based algorithm can be applied to detect which of these components are connected to the exterior, and, therefore, the *Effective Porosity* can be estimated as the number of empty voxels of

these components. In order to compute the radial distribution of pores, virtual pores must be fitted into the empty space. Several methods to do so have been proposed. Some authors count only one pore per connected component of the empty space [12]. Other authors [2] [13] consider as pores maximal disjoint spheres centered in the skeleton of the pore space. Even if these methods give visually good results, it is difficult to validate them in comparison to physical measures, because they are not based on the porosimeter principle.

Connectivity is another interesting structural parameter that characterizes the mechanical properties of a trabecular bone or a bio-implant. It can be computed from the Euler characteristic [6] and also by representing the sample in a plate/rod model [10]. Connectivity computation is beyond the scope of this work and is part of the future work.

In this paper, we propose a new method to simulate the behavior of the porosimeter using microCT 3D images of a bio-implant. Our method is based on an iterative process of virtual intrusion into the pore space. It obtains results comparable to those of the real porosimeter. Moreover, it provides information of pore adjacency in the pore space and of the pores that are not connected to the exterior. In addition, it can be compared to other pores fitting methods in order to evaluate their assets and flaws.

2. BACKGROUND

2.1 Porosity Characterization

A porous material can be defined as a solid material with holes in it [4]. In a porous material as a bioimplant, we consider the volume of the solid phase, V_b and the volume of the porous phase, V_p . The *Total Porosity* is defined as the volume fraction of the porous phase, $TP = (V_p / (V_p + V_b))$. In the porous phase, two different types of regions are considered, the porous regions connected with the exterior (with volume V_{ext_p}) and the isolated regions not connected with the exterior and referred as cavities. The *Effective Porosity* is related to the first kind of regions, $EP = (V_{ext_p} / (V_p + V_b))$. We also consider the surface area as the area of the surface between solid and porous phase.

Properties of the pore space are pore size and shape. In materials presenting a porous topology with cavities completely isolated, each cavity is considered a pore and, therefore, it is easy to obtain a pore size distribution. But for the most usual topologies, with a porous phase fully connected, it is more difficult to characterize shape and size of the pores and several approaches use the concept of throat. The size of a throat limits the accessibility of a possible larger pore, and for material properties as permeability, is the size of importance and a pore throat size distribution can be computed. The physical experiments based on porosimetry and the approach presented in this paper that simulates them are based on the concept of throat.

2.2 Porosity Measurement with a Porosimeter

Porosimetry is based on the capillarity law governing penetration of non-wetting liquid as mercury into porous regions. Experiments with a porosimeter allow to intrude mercury at different pressures, obtaining the corresponding intruded volumes.

Porosimetry measurements generates a mapping between the real pore structure and a random network of cylindrical tubes with circular section. This mapping is useful for calculating several parameters as porosity and fluid permeability, but not for a real geometric representation of the pore structure. Although it would be better to consider pores with elliptical cross-section, the results based on circular cross-section for these parameters are equivalent [3]. Due to the nature of this experiment, only porous regions connected with the exterior are considered.

Considering cylindrical pores, the Washburn equation gives a representative diameter for each pressure, $D = \sqrt{4 WC \gamma \cos \varphi} / P$, where D is the diameter, P is the applied pressure, γ is the surface tension, φ is the contact angle and WC is the Washburn constant.

Then, for each intruded pressure P_i , the porosimeter gives the corresponding intruded volume, V_i . It also computes the specific volume $I_i = V_i / W_s$, W_s being the weight sample. Diameter D_i corresponding to pressure P_i is computed by the Washburn equation. Then, each incremental specific volume, computed as $\Delta I_i = I_i - I_{i-1}$, is associated to the corresponding mean diameter, $D_{mi} = (D_i + D_{i-1})/2$ and to the incremental specific pore area $\Delta A_i = 4 \Delta I_i / D_{mi}$, for each applied pressure.

2.3 Bio-CAD Methods for Porosity Estimation

Recently several methods have been developed to measure structural parameters as porosity and connectivity from digital images. Concerning with the porosity, there are methods that simply compute TP from the voxelized model by simple voxel counting [11] [12].

Devising a complete representation of the pore space is addressed in very few papers. In [12], a pore is defined simply as a 6-connected component of the pore space. The pore space is subdivided into connected components and each of them is considered a pore. The surface of the pores is extracted using the Marching Cubes (MC) triangularization. In this work, the authors conclude that, since the pore space is generally highly connected, in most cases, they detect only one pore. A more precise modeling of the pore space is performed in [2] in order to evaluate the permeability and pore size parameters. This method is based on an initial skeletonization of the pore space and the application of a two-pass heuristic. First, the pore space is filled with non-overlapping spheres centered at skeleton points, and, then, these spheres are inflated until any voxel of the pore space belongs to one of them. These inflated spheres are considered individual pores. However, this method can create pores with strange shapes, that may have local narrowings.

Another approach computes a graph of the pore space such that each node of the graph represents a pore, and an edge between two nodes indicates that the two pores are path-connected [13]. In this approach, pores are disjoint and with maximal sizes. This method separates the porous region into connected components and applies a four-step process to each of them. After computing the distance map, the method identifies local maxima in it and computes a rasterized sphere associated to each local maxima. Initially, every rasterized sphere is considered as a potential pore and, therefore, pores can share voxels. The method supports a data structure with all the sets of voxels belonging to each possible pore (non-shared with other pores) and to each combination of interfering pores (shared voxels). The third step allows to grow some pores, shrink others and remove other ones so that, at the end of the step, all the remaining pores are disjoint. The applied criterion is based on the size of the non-shared and shared subsets of pores. The four step computes the arcs of the graph.

Other techniques to compute porosity are based on stochastic geometry (Monte Carlo methods) [9] and fractal analysis [7].

3. THE VIRTUAL POROSIMETER

3.1 Overview

The method presented in this paper is composed of four main steps: segmentation, computation of the connected components of the pore space, porosimeter simulation and construction of the pores interconnectivity graph. The first two steps are common to other BioCAD methods for the estimation of porosity.

In the first step, we classify the voxel model into three regions: V_e (exterior), V_b (biomplant) and V_p (pore space). Once the model has been segmented, we are able to compute the *Total Porosity (TP)* on the basis of the number of voxels of the pore space in relation to the number of voxels of the material: $TP = |V_p| / (|V_p| + |V_b|)$.

In the second step, we separate the pore space into its set of connected components CP_i $i=1 \dots n$ using a customized connected component labeling algorithm [5] that scans the volume slice to slice, updating a list of 26-connected components. Next, we check for each of the components if there exists at least one voxel of the component that is connected to the exterior. The set of the connected components connected to V_e is $Vext_p$. Then the *Effective Porosity* is computed as:

$EP = |Vext_p| / (|V_p| + |V_b|)$. In this step of the process, we compute a voxel model of the sample such that each voxel is labeled according to the connected component to which it belongs.

The third step of the process, described in Section 3.2 consists of the simulation of the porosimeter. It takes as input the labeled voxel model computed in the second step and gives as output a new voxel model such that each voxel is labeled according to the virtual pressure with which the voxel has been virtually filled. The radial distribution of the pores is computed on the basis of the incremental volumes filled at different virtual pressures.

Finally, the fourth step, constructs the pores interconnectivity graph using the voxel model computed in step three. This is explained in Section 3.3.

3.2 Simulation of the Porosimeter

The presented approach follows a brute force strategy that simulates the incremental penetration of mercury at increasing pressures. As in real porosimetry only those connected components connected to the exterior (reachable components) are able to be filled, so totally interior components (cavities) won't be considered.

The input of this process is the voxel model, labeled by its connected components, and with its associated distance map and a list of decreasing radii, r_1, r_2, \dots, r_n . This list of radii can be computed from the corresponding given pressures, by applying the Washburn equation, or by defining intervals between the minimum and maximum values of the distance map. As we are simulating the porosimeter, we will obtain this list with the same pressures used in the real porosimeter. Each of these radii, r_i , actually represents the radii interval $[r_i, r_{i+1}[$, so we will refer to them as *intrusion radius interval*. The output of the process is the connected component with its voxels labeled with the maximum *intrusion radius interval* (or the corresponding virtual pressure) that has allowed to fill it.

The algorithm performs the following process for each reachable connected component. First, it computes its skeleton, using the method presented in [8] and [1], which obtains a surface (2D) skeleton with the same connectivity as the original model. Then, it identifies those skeleton voxels that are connected with the exterior and initializes a list (*globalseed list*) with them.

After these two initial processes, the iterative process for each *intrusion radius interval* is performed in descending radius order. First, all those voxels in the *globalseed list* with a value belonging to the current *intrusion radius interval* are inserted into another list (*currentseed list*) as seed voxels for the simulation of the filling process corresponding to the current iteration.

Then, for each voxel of the *currentseed list*, a sphere centered at this voxel and with a radius equal to the voxel associated distance is considered and all those voxels inside it are labeled with the current *intrusion radius interval*, except those already labeled in a previous iteration. When all the voxels in the *currentseed list* have been processed, the method continues with their neighbors. Therefore, all those skeleton voxels which are neighbors of a processed seed voxel are considered. Those with a value belonging to the current *intrusion radius interval* and that have not already been processed as a seed are inserted into the *currentseed list* while those with a value not belonging to the current *intrusion radius interval* (a smaller value) are inserted in the *globalseed list* and will be processed in their corresponding iteration. Note that all those voxels not corresponding to the current *intrusion radius interval* have not yet been processed as a seed.

When the *currentseed list* is empty and all the processed neighbors have a value not belonging to the current *intrusion radius interval*, the method performs the following iteration corresponding to the next *intrusion radius interval*. Then, all those voxels in the *globalseed list* with a value belonging to this next *intrusion radius interval* are inserted into the *currentseed list* and the process continues in the same way as the previous iteration until both lists, *currentseed* and *globalseed*, are empty. To facilitate this process the *globalseed list* is sorted by the *intrusion radius interval*. Fig. 1 illustrates the algorithm.

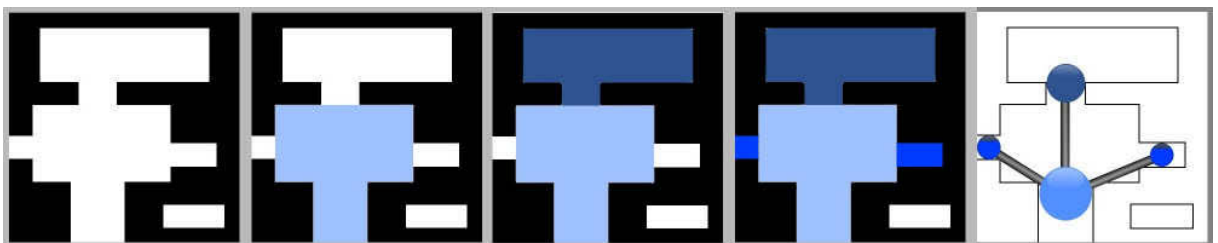


Fig. 1: Example of three iterations with the virtual porosimeter. From left to right: The original voxel model; First iteration at the smaller intrusion pressure P_1 ; Second iteration at a stronger intrusion pressure P_2 ; Third iteration at the strongest intrusion pressure P_3 : All reachable voxels are now labeled; The computed pore graph. Note the isolated cavity in white.

3.3 Pores Interconnectivity Graph Computation

We construct a graph of the pores interconnectivity such that the nodes of the graph are the pores computed with the porosimeter simulator, and such that an edge between two pores p_i and p_j indicate that p_i and p_j are directly path-connected, i.e., there exists at least one voxel v_i of p_i and one voxel v_j of p_j that are adjacent.

After the porosimeter simulation, each connected component of the pore space is composed of pores with different labels. We apply the same connected component labeling [5] as the one used in the second step of the overall process. This gives us a list of all the voxels associated to each pore. We use this list to construct the pores graph by inserting the pores as nodes of the graph. We associate to each node the intrusion pressure of the pore, its minimum and maximum radii computed as the minimum and maximum value of the distance map of the pore's voxels, its set of voxels and the minimum bounding box of the set. Finally, we check the neighbor voxels of all the voxels of each node of the graph, and insert an edge in the graph between the nodes that have adjacent voxels.

The volume of a pore is computed as the sum of volumes of its corresponding voxels. An alternative way to compute it is from its boundary, represented with the MC extracted triangular surface.

The graph can be used to query for any pair of pores if they are path-connected and which is the minimum radius of the connection. To do so, we just have to traverse the graph starting at the node corresponding to one pore until reaching the node corresponding to the other and updating through the path the minimum radius.

Moreover, the graph pore can be visualized, as illustrated in Fig. 1. Each node is represented by a sphere proxy having as center the center of its minimum bounding box and as radius the one corresponding to its intrusion pressure. Each edge is represented by a segment between the two pores minimum bounding boxes centers.

4. EXPERIMENTAL RESULTS

We have applied the presented method on different models. We first show in Fig. 2 a set of four frames of the animation of the virtual porosimeter process inside a femur bone sample.

We herein show the results obtained on a sample (dataset 1) of Poly-95%LL,5%DL-lactic acid (PLA). Fig. 3 shows a slice of this model. The scanned images have a resolution of 1750x1750x501 with a voxel's edge size of 0.7 μ m. Since the volume data is huge, we have downsampled the images to a more amenable size of 256x256x73 using a trilinear interpolation filter. Then, we have applied a threshold filter to binarize the images. Next, we have segmented the model into three regions: the exterior empty space, the material and the internal empty space, i.e. the porous region. Since the sample is a cylinder, we have been able to implement this segmentation as a geometric process of clipping the images against a circular shape. Then, we have applied a median filter to remove the salt-and-pepper noise of the images. Finally, we have applied the explained porosimeter simulation to the images.

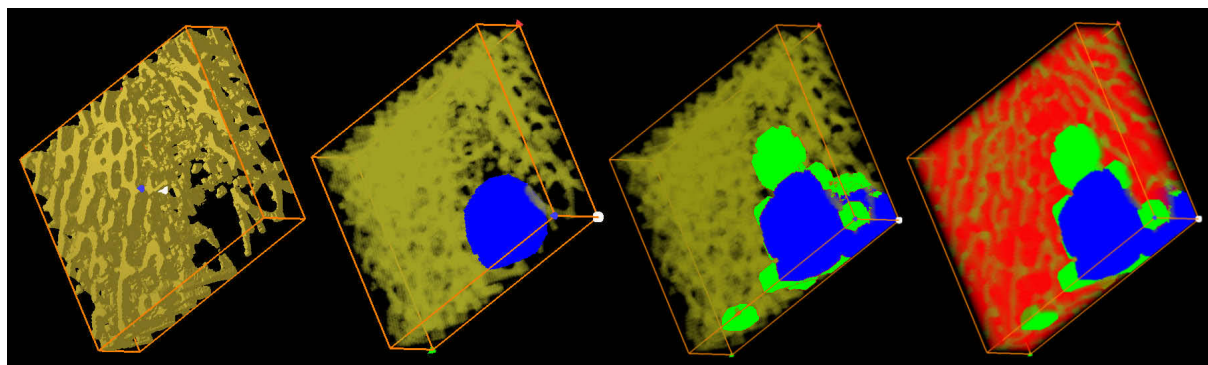


Fig. 2: Four steps of an animation of the filling process. From left to right: Initial bone mesh; First intrusion is shown in blue; Second intrusion iteration in green; Last intrusion in red. All pore space voxels are reached.

We have applied the proposed method to another sample (dataset 2) of the same material with size 1280x1280x987 and a voxel size of 7.56 μm . This dataset has been downsampled and sliced to 1024x1024x96. We have been supplied with the real porosimeter's histogram for this sample, so we have obtained the histogram with the proposed method for the downsampled dataset (See Fig. 4). The results compared with those of the porosimeter's are very similar. The differences are due on one hand to the discretization of the sample in the scanning process and the loss of information due to the downsampling; on the other hand to the fact that the some mercury is stuck on the pores surface in the porosimeter and blocks some small throats. In the histogram, we show the volumes computed as the sum of volumes of its corresponding voxels. We have also computed them by using the surface generated with MC and the volumes are more fitted to the connected components but similar to the voxel counting approach. The differences between the volumes computed in both methods are less than 15%, depending on the size and shape of the connected components.

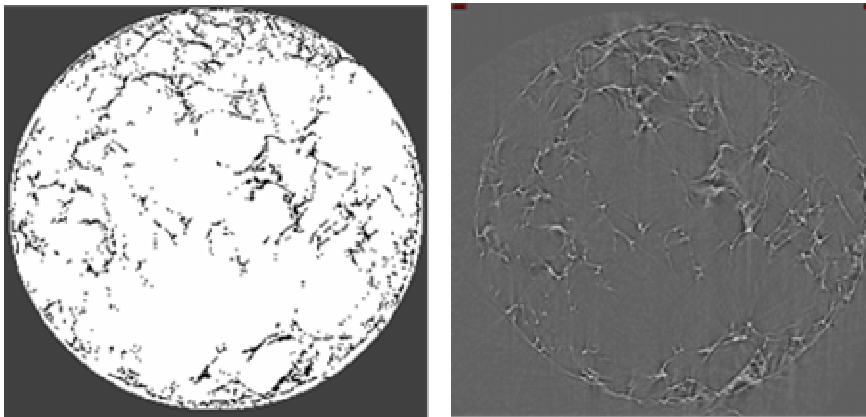


Fig. 3: A slice of the dataset 1 before (left) and after (right) pre-processing. In the left image the bioimplant is white and the empty region is gray. In the right image, the dark gray voxels are exterior, the black ones are the biomaterial and the white the empty ones.

We can also compare the TP obtained with our method and from the microCT reported values. From dataset 2, the microCT report provides TP=97.718% and we have computed TP=97.485%.

In Fig. 5 (right) a 3D image of dataset 1 is shown where each voxel of the porous region has been colored according to its corresponding intrusion pressure. Fig. 5 (left) shows a 2D cross section of the same model. We can observe the spherical shape of the “waves front” filling the porous region.

The real porosimeter does not separate regions labeled with the same intrusion pressure into different cavities according to their radii (see Fig. 6). The Virtual Porosimeter obtains the same result. Geometric-based methods for the estimation of pores do take into account the topology of the porous region, and therefore, they obtain a different, more accurate representation of the porous region taken into account the reachable components as well as the cavities. We can see the differences between the two models. The comparison of the results of the geometric method and the Virtual Porosimeter results allows us to check the validity of the geometric method.

5. CONCLUSIONS AND FUTURE WORK

We have presented a new method to simulate the measurements of a porosimeter onto a BioCAD voxel model of a CT scanned bio-implant. Our method consists of iteratively flooding the empty region inside the bioimplant through increasing intrusion radii. We achieve a good simulation of the real porosimeter. Moreover, we are able to compute and visualize a pores interconnectivity graph. The method allows us to validate other pores estimation methods based on geometric and topological properties of the empty region. As the global process of the image is costly, we are currently working on enhancing its efficiency optimizing the algorithms. Moreover, we are studying and developing methods to compute other structural parameters of trabecular bone and bio-implants such as connectivity and anisotropy.

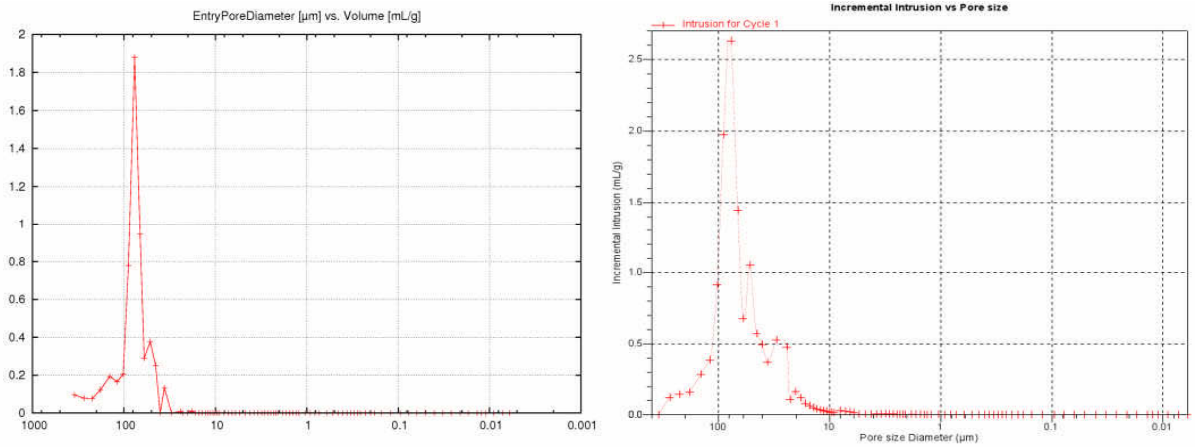


Fig. 4: The computed histogram for dataset 2 (left) compared to the real porosimeter one (right). The X-axis (log) shows the entry pore diameter (in μm), the Y-axis the volume filled (in mL/g).

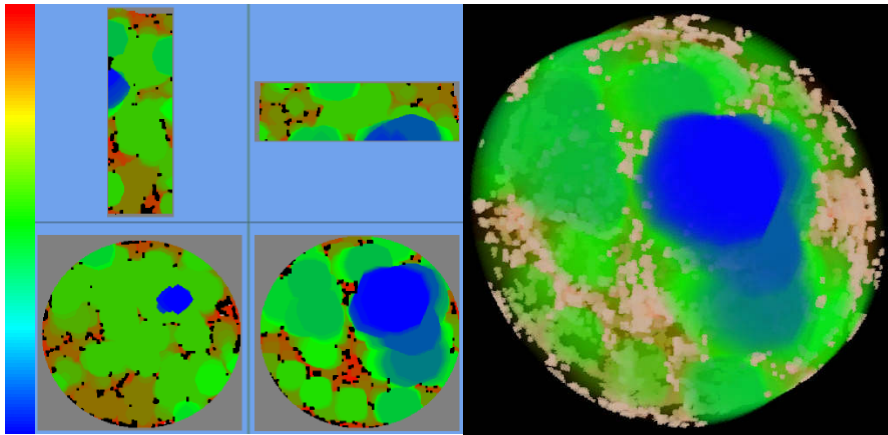


Fig. 5: Four different 2D cross sections of the filled pores for dataset 1 (left). 3D visualization of this model (right). The color scale symbolizes the filling pressure (blue for low pressure and high entry size, red for high pressure and low entry size). The material is shown in black (left) and pink (right).

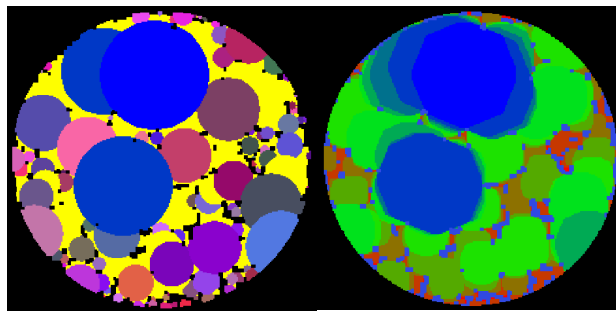


Fig. 6: Pores computed for dataset 1 (applying the geometric-based pore fitting method [13] (left) and the proposed porosimeter simulation method (right).

6. ACKNOWLEDGMENTS

This work has been partially funded by the project MAT2005-07244-C03-03 and the project 02-1/07 of the Institut de Bioenginyeria de Catalunya (IBEC).

7. REFERENCES

- [1] Ayala, D.; Vergara, E.; Vergés, E.: Improved skeleton computation of an encoded volume, Proc. of Eurographics 2007, 2007, 33-36.
- [2] Cleynebreugel, T. V.: Porous scaffolds for the replacement of large bone defects, A biomechanical design study, PhD thesis, Katholieke Universiteit Leuven, 2005.
- [3] Garboczi, E. J.: Mercury porosimetry and effective networks for permeability calculations in porous materials, Powder Technology, 67, 1991, 121-130.
- [4] Garboczi, E. J.; Bentz, D. P.; Martys, N. S.: Digital images and computer modeling, In Experimental methods in the physical Sciences, 35, Methods in the physics of porous media, Academic Press, 1999, 1-41.
- [5] Grau, S.; Ayala, D.; Tost, D.; Miño, N.; Muñoz, F.; González, A.: In-silico evaluation of bone implants, Proc. of CEIG'05, 2005, 245-248.
- [6] Martín-Badosa, E. et. al.: A method for the automatic characterization of bone architecture in 3D mice microtomographic images, Comp. Medical Imaging and Graphics, 27, 2003, 447-458.
- [7] Polyakov, V.; Kucheryavskii, S.: The fractal analysis of a porous material structure, Technical Physics Letters, 27(7), 2001, 592-593.
- [8] Rodríguez, J.; Thomas, F.; Ayala, D.; Ros, L.: Efficient Computation of 3D Skeletons by Extreme Vertex Encoding, Proc. Discrete Geometry for Computer Imagery, 11th Int. Conf. Springer, 2003, 338-347.
- [9] Schroeder, C.; Regli, W. C.; Shokoufandeh, A.; Sun, W.: Computer-aided design of porous artifacts, Computer-aided design, 37, 2005, 339-353.
- [10] Stauber, M.; Müller, R.: Volumetric spatial decomposition of trabecular bone into rods and plates - A new method for local bone morphometry, Bone, 38, 2006, 475-484.
- [11] Tuan, H. S.; Hutmacher, D. W.: Application of micro CT and computation modeling in bone tissue engineering, Computer-Aided Design, 37(11), 2005, 1151-1161.
- [12] Vanis, S.; Rheinbach, O.; Klawonn, A.; Prymak, O.; Epple, M.: Numerical computation of the porosity of bone substitution materials from synchrotron micro computer tomographic data, Materialwissenschaft und Werkstofftechnik, 37(6), 2006, 469-473.
- [13] Vergés, E.; Ayala, D.; Grau, S.; Tost, D.: 3D reconstruction and quantification of porous structures. Proc. of CEIG'07, 2007, 179-186